Trotter-number scaling in Monte Carlo studies of the small polaron

1997 J. Phys.: Condens. Matter 9 10675

(http://iopscience.iop.org/0953-8984/9/48/011)

J. Phys.: Condens. Matter **9** (1997) 10675–10685. Printed in the UK PII: S0953-8984(97)84536-5

Trotter-number scaling in Monte Carlo studies of the small polaron

Pavel Kornilovitch

Max-Planck-Institut für Physik komplexer Systeme, Noethnitzer Strasse 38, D-01187, Dresden, Germany

Received 27 May 1997, in final form 30 September 1997

Abstract. A path-integral quantum Monte Carlo method is applied to the two-dimensional single-polaron Holstein model. Simulation data are shown to exhibit $1/M^2$-scaling with the number of imaginary-time slices M used in the Trotter decomposition. Numerical extrapolation to $M \to \infty$ yields very accurate estimation of polaron energetic characteristics. Kinetic, potential and total energy are calculated as functions of the electron–phonon coupling strength for different phonon frequencies. The small-polaron regime is found in the strong-coupling limit for all of the frequencies studied. The transition to the polaron state is sharp in the adiabatic regime but broadens as the frequency increases. In the adiabatic limit the polaron forms at $\lambda_{cr} = 0.80 \pm 0.05$.

1. Introduction

The basic properties of the small polaron are well established; see the reviews [1–6] and the references therein. However, the lack of an exact solution continues to prompt new research, especially in the parameter regions not accessible to the various perturbative techniques. In the last decade the polaron problem attracted additional attention in connection with high-temperature superconductivity [7–9]. In the cuprates the electron kinetic energy is suppressed due to strong correlations. On the other hand, the electron–phonon (EP) interaction is found to be strong [7]. Therefore the potential energy of the EP interaction could be comparable with the kinetic energy which may lead to the formation of small polarons. Although in this respect the many-polaron problem is the main interest, the single-polaron one is the necessary first step.

With the dramatic progress in computer performance in the last two decades new computational approaches to the old problem have been developed. The most popular method is the exact diagonalization (ED) of Hamiltonian matrices. It allows one to compute static as well as dynamic physical properties with very high accuracy and thereby provides exact and unbiased information about the polaron properties. The ED method has been exploited by a number of groups [10–14]. The main limitation of this approach is its restriction to very small clusters. The Hilbert space of an EP model is infinite, even for a finite number of lattice sites, since the number of phonons is not conserved. Usually in ED studies the Hilbert space is truncated in such a way that the total number of phonons is limited to some number n_{max}. With a typical $n_{max} = 50$ the maximum number of sites feasible is a modest four [11–13]. Then one hopes that polaron properties obtained on such a small cluster are reasonably close to the bulk limit. This is true for such quantities as the ground-state energy or the local EP correlation function, especially in models with local EP

0953-8984/97/4810675+11$19.50

interaction like Holstein or Su–Schrieffer–Heeger models. However, this is definitely not so, for instance, for the effective mass, which requires the knowledge of the ground-state energy for infinitesimally small momenta absent on a finite lattice. Moreover, the exact-diagonalization approach suffers from either a finite-size effect or poor n_{max}-convergence in the following cases: (i) in the band-electron regime but close to the small-polaron crossover, where the size of the phonon cloud is still large; (ii) in models with long-range EP interaction; (iii) in the adiabatic regime when the number of excited phonons is large [11]. Recently developed ED-related techniques such as the variational Lanczos [15], numerical strong-coupling renormalization [16] and density-matrix [17] ones are still non-universal although they are an advance beyond the traditional ED scheme. Another fundamental limitation of all of the methods mentioned is their restriction to the ground-state properties. No finite-temperature algorithm, so important for the comparison with experiments, has been developed so far.

An alternative numerical approach to the polaron problem is the quantum Monte Carlo (QMC) method based on the mapping of a d-dimensional quantum system to a $(d+1)$-dimensional classical one and the subsequent application of standard Monte Carlo algorithms. The traditional QMC scheme, which applies to the general many-polaron case, amounts to simulating both the electron and phonon subsystems [18–21]. For the single-polaron problem a much more efficient algorithm was developed by De Raedt and Lagendijk (DRL) in 1982 [22]. It stems from the observation that in the single-electron case the majority of degrees of freedom in a path-integral representation of a partition function are phononic. The latter, however, can be integrated out analytically with Feynman's technique [23, 24] without making any approximation. The resulting system is a single electron which interacts with itself via a retarded potential. Thus, DRL's method follows the strategy which proved so successful in the studies of the continuum Fröhlich polaron [23, 2, 25]. The only difference is that the self-interacting electron is treated numerically by the Metropolis algorithm [26] rather than variationally.

It is quite remarkable that DRL's method lacks *any* of the shortcomings of the exact-diagonalization approach, mentioned above. It is independent of the lattice size and dimensionality and of the form of the electron kinetic energy. It is temperature dependent, the inverse temperature entering the formalism as the extent of the extra imaginary-time dimension. It is equally well suited for studying different parameter regions including intermediate phonon frequencies and coupling constants. The general idea of the method is applicable to any type of phonon spectrum and EP interaction as long as the latter is linear in phonon coordinates and the lattice is harmonic. Actual simulations, however, were performed only for local EP interaction without [22] and with [27] phonon dispersion. It differs from other QMC schemes in that the polaron contribution is separated analytically from the lattice one and hence the polaron properties are not obscured by the statistical noise of the phonon subsystem.

Therefore it is surprising that since the pioneering work of DRL on the Holstein polaron [22, 27] (see also [28]) and bipolaron [29] very little has been done to develop the method further. The only recent development is the calculation of the polaron effective mass [30]. One might suspect that the numerical accuracy of the method is not good enough to provide quantitative information about the system. It is the aim of this paper to demonstrate that this is not the case. In fact, energetic characteristics can be calculated with accuracy better than 10^{-2} of the bare electron kinetic energy. This is sufficient for practical purposes, in particular for establishing phase boundaries. The crucial device here is to make use of the specific scaling that the Monte Carlo data exhibit with the change of the number of imaginary-time slices (see below). With this development the QMC method becomes able

to provide not only qualitative but also accurate quantitative information about the polaron. We will also present numerical results for the two-dimensional Holstein model for different frequency regimes.

2. Theoretical formalism

In this paper the small polaron is studied in the framework of the Holstein model [31]. In its simplest version the model describes an electron moving in a lattice composed of molecules which do not interact with each other. We will consider the two-dimensional square lattice with periodic boundary conditions. With each lattice site is associated a single local vibrational mode, i.e. the molecules may be viewed as harmonic oscillators with frequency ω and reduced mass m. Since the oscillators are not coupled, the phonons are dispersionless. The electron moves through the lattice by means of hops between nearest oscillators, with the hopping matrix element $-t$. The interaction is chosen in the form 'density–local displacement' which means that the electron interacts only with the oscillator that it currently occupies and the interaction energy is proportional to the displacement ξ of the oscillator from its equilibrium position. The model Hamiltonian reads

$$H = H_e + H_{ph} + H_{e-ph} = -t\sum_{\langle ij\rangle} a_i^\dagger a_j + \frac{1}{2m}\sum_i p_i^2 + \frac{m\omega^2}{2}\sum_i \xi_i^2 + g'\sum_i a_i^\dagger a_i \xi_i \qquad (1)$$

where i numbers lattice sites, a_i ($a_i^\dagger$) is the electron destruction (creation) operator, $p_i = -\mathrm{i}\hbar\,\partial/\partial\xi_i$ and g' is the EP coupling constant. This coupling constant has the dimensionality of force and its sign is irrelevant. Very often the electron–phonon interaction is introduced in a different form:

$$H_{e-ph} = g\hbar\omega\sum_i a_i^\dagger a_i (b_i^\dagger + b_i) \qquad (2)$$

where $b_i^\dagger$ and b_i are phonon operators. The coupling constants g and g' are related as follows:

$$g = \frac{g'}{\sqrt{2m\hbar\omega^3}}. \qquad (3)$$

Two more quantities are useful in the description of the polaron problem. The first one is the polaron shift E_p which characterizes the potential energy of the EP interaction. The second one is the ratio λ of E_p and the bare half-bandwidth of a free electron. With g and g' as defined above, one has

$$E_p \equiv g^2\hbar\omega = \frac{g'^2}{2m\omega^2} \qquad \lambda \equiv \frac{2E_p}{W} = \frac{g'^2}{2ztm\omega^2} \qquad (4)$$

where z is the number of nearest neighbours ($z = 4$ for the square lattice). Note that both E_p and λ are independent of m, since $\omega \propto m^{-1/2}$.

In the rest of this section we present the necessary formulae of the path-integral QMC method due to De Raedt and Lagendijk [22]. The partition function of the system is approximated by the Trotter formula [32, 33]

$$\begin{aligned} Z \equiv \mathrm{Tr}\left\{\mathrm{e}^{-\beta H}\right\} &= \lim_{M\to\infty} Z_M \\ &= \lim_{M\to\infty} \mathrm{Tr}\left\{\left(\exp\left(-\frac{\beta}{M}H_e\right)\exp\left(-\frac{\beta}{M}H_{ph}\right)\exp\left(-\frac{\beta}{M}H_{e-ph}\right)\right)^M\right\} \end{aligned} \qquad (5)$$

where $\beta = 1/k_B T$ is the inverse absolute temperature and $M \gg 1$ is the number of imaginary-time slices introduced. Inserting the resolution of the identity $M-1$ times and evaluating the matrix elements of the operators $\exp(-(\beta/M)H_e)$, $\exp(-(\beta/M)H_{ph})$ and $\exp(-(\beta/M)H_{e-ph})$ one obtains

$$Z_M = c_1 \sum_{\{\boldsymbol{r}_j\}} \int_{-\infty}^{\infty} \left[\prod_{i=1}^{N^2} \prod_{j=0}^{M-1} \mathrm{d}\xi_{ij} \right] \mathrm{e}^{-S_{ph}} \left[\prod_{j=1}^{M} I(\boldsymbol{r}_{j+1} - \boldsymbol{r}_j) \right]. \tag{6}$$

Here the new index j numbers imaginary-time slices introduced by the decomposition (5), $j = 0, \ldots, M-1$. Accordingly, $\boldsymbol{r}_j$ is the position of the electron and ξ_{ij} the displacement of the ith oscillator in the jth time slice. The function I represents the electron kinetic energy:

$$I(\boldsymbol{r}_{j+1} - \boldsymbol{r}_j) = \frac{1}{N} \sum_{\boldsymbol{k}} \exp(\mathrm{i}\boldsymbol{k} \cdot (\boldsymbol{r}_{j+1} - \boldsymbol{r}_j)) \exp(2\tau(\cos k_x + \cos k_y)) \tag{7}$$

with $\tau \equiv \beta t/M$ and N the total number of lattice sites. S_{ph} in equation (6) is the phonon action

$$S_{ph} = \sum_{i=1}^{N} \sum_{j=0}^{M-1} \left[\frac{m}{2\tau\hbar^2} (\xi_{i,j+1} - \xi_{ij})^2 + \tau \frac{m\omega^2}{2} \xi_{ij}^2 - \tau g' \xi_{ij} \delta_{i,x_j} \right] \tag{8}$$

which is a quadratic form in oscillator coordinates. Therefore the integral over ξ_{ij} in equation (6) can be performed analytically with Feynman's technique [23, 24] leading to the final result

$$Z_M = c_2 Z_M^{ph} Z_M^F \qquad Z_M^F = \sum_{\{\boldsymbol{r}_j\}} \rho(\{\boldsymbol{r}_j\}) \tag{9}$$

$$\rho(\{\boldsymbol{r}_j\}) = \left[\prod_{j=1}^{M} I(\boldsymbol{r}_{j+1} - \boldsymbol{r}_j) \right] \exp\left(\sum_{j,j'=0}^{M-1} \delta_{\boldsymbol{r}_j, \boldsymbol{r}_{j'}} F(j - j') \right) \tag{10}$$

$$F(j - j') = \frac{\tau^3 g_1^2}{4M} \sum_{l=0}^{M-1} \frac{\cos[(2\pi l/M)(j - j')]}{1 - \cos(2\pi l/M) + \tau^2 \omega_1^2/2}. \tag{11}$$

Here c_2 is an unimportant constant and Z_M^{ph} is the partition function of free bosons, which can be calculated exactly and is not of interest. The fermionic partition function Z_M^F is a sum over all possible trajectories $\{\boldsymbol{r}_j\}$ which are periodic in imaginary time, i.e. $\boldsymbol{r}_M = \boldsymbol{r}_0$. Each trajectory contributes its weight $\rho(\{\boldsymbol{r}_j\})$, equation (10), which consists of a kinetic energy factor and the one from the retarded self-interaction. This self-interaction is mediated by phonons and characterized by the memory function $F(j - j')$, equation (11). The dimensionless phonon frequency ω_1 and coupling constant g_1 appearing in $F(j - j')$ are related to the model parameters as follows:

$$\omega_1 \equiv \frac{\hbar\omega}{t} \qquad g_1^2 \equiv \frac{\hbar^2 g'^2}{mt^3} = 2g^2\omega_1^3 = 2z\omega_1^2\lambda. \tag{12}$$

The partition function is of no interest by itself but its derivatives are. In particular, the internal energy may be obtained from the thermodynamic relation $U = -\partial(\ln Z)/\partial\beta$. Applying it to equations (10) and (10) one discovers (apart from the energy of free phonons) two terms, one resulting from the kinetic part of $\rho(\{\boldsymbol{r}_j\})$ and another from the interaction

$$\frac{1}{t} U_M^F = K_M^F + P_M^F \tag{13}$$

$$K_M^F = -\frac{1}{M}\sum_{j=0}^{M-1}\sum_{\boldsymbol{l}}\left\langle \frac{I(\boldsymbol{r}_{j+1}-\boldsymbol{r}_j+\boldsymbol{l})}{I(\boldsymbol{r}_{j+1}-\boldsymbol{r}_j)}\right\rangle \tag{14}$$

$$P_M^F = -\frac{1}{M}\sum_{j=0}^{M-1}\sum_{j'=0}^{M-1}\frac{\partial F(j-j')}{\partial\tau}\left\langle \delta_{\boldsymbol{r}_j,\boldsymbol{r}_{j'}}\right\rangle . \tag{15}$$

Here $\boldsymbol{l}$ runs over four nearest neighbours of the square lattice and the following definition is introduced:

$$\langle A\rangle \equiv \frac{1}{Z_M^F}\sum_{\{\boldsymbol{r}_j\}} A(\{\boldsymbol{r}_j\})\rho(\{\boldsymbol{r}_j\}). \tag{16}$$

K_M and P_M are the average polaron kinetic and potential energy respectively.

3. The simulation procedure

Due to the complicated structure of the memory function $F(j-j')$, the averaging of (16) cannot be done analytically. However, one can use the Metropolis algorithm [26] which is well suited for the calculation of this type of average. Details of the algorithm are well known and can be found in the literature [28, 34]. It is very important that after the elimination of phonons the simulated system contains one degree of freedom only. Therefore the transition from one member of the Markov sequence to the next requires a small amount of calculation. This fact allows one to accumulate a large set of statistics within reasonable computational time. In this work as many as $\sim 2\times 10^8$ single steps were performed for every set of model parameters which however required only a few hours of CPU time of a modern workstation. Also due to the single-degree-of-freedom property the size of the lattice is absolutely irrelevant. It does not affect the computational time and simulation results saturate after approximately $N = 8\times 8$. In this work a lattice of $N = 32\times 32$ sites was studied.

It is important that Trotter decomposition (5) is approximate for any finite number of imaginary-time slices M. In practice, simulations can be done at finite M thereby yielding only approximations to true results. The question therefore is that of how large M needs to be for the simulation results to be reliable. Let α be the largest energetic parameter of the model, i.e. $\alpha = \max\{t, \hbar\omega, g'\sqrt{\hbar/m\omega}\}$, and $x \equiv \beta\alpha/M$. Then one has

$$\exp\left(\frac{\beta}{M}H\right) = \exp\left(\frac{\beta}{M}H_e\right)\exp\left(\frac{\beta}{M}H_{ph}\right)\exp\left(\frac{\beta}{M}H_{e-ph}\right) + \mathcal{O}(x^2) \tag{17}$$

since $H_e + H_{ph}$ and H_{e-ph} do not commute. The total partition function is a product of M operators of type (17). Thus one might expect the accuracy of the whole scheme to be $\mathcal{O}(x\beta\alpha)$. If fact, the accuracy of action (8) and all of the rest of the formalism is much higher. The reason for this is the commutativity of H_{e-ph} with the operators projecting on the real-space electron–phonon configurations used as basis states. Therefore equation (17) is equivalent to the symmetric decomposition

$$\exp\left(\frac{\beta}{M}H\right) = \exp\left(\frac{\beta}{2M}H_{e-ph}\right)\exp\left(\frac{\beta}{M}H_e\right)\exp\left(\frac{\beta}{M}H_{ph}\right)\exp\left(\frac{\beta}{2M}H_{e-ph}\right) + \mathcal{O}(x^3) \tag{18}$$

known to be correct up to x^3 [28]. Thus, the formulae of the previous section are correct up to $\mathcal{O}(x^2\beta\alpha)$. Usually the values of M are chosen intuitively on the basis of the condition $x^2\beta\alpha \ll 1$ [18–20]. But in this case the corrections to true results remain uncertain because

the prefactor is unknown. The efficiency of the present algorithm enables us to study the M-convergence of the QMC data systematically and to make use of the $1/M^2$-scaling that the data are expected to exhibit. This amounts to simulating the system at several different values of M and the extrapolation of the results to $M \to \infty$.

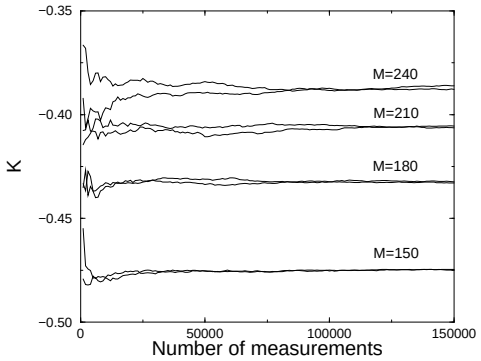

Figure 1. The running average for the polaron kinetic energy for $\beta = 15t^{-1}$, $\omega_1 = 0.3$, $g_1 = 1.5$ for different values of M. The results scale as $1/M^2$. The lattice size is 32×32.

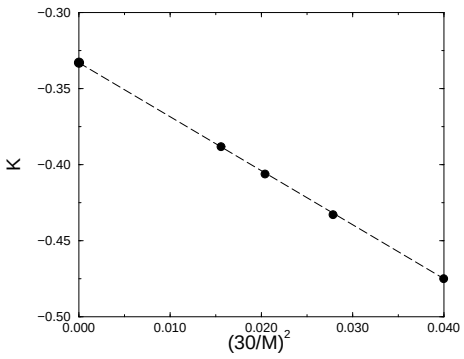

Figure 2. The extrapolation of the data of figure 1 to the $M = \infty$ limit. The accuracy of the $M = 150$, $\tau = 1/10$ result (the point on the far right) is 40%.

One should expect different behaviours depending on which of the three energy parameters is the largest one. For small ω_1 and g_1 the electron hopping integral is the largest, and hence $\alpha = \tau = \beta t/M$. In this case no significant M-dependence is observed starting with $M = 90$ (for the inverse temperature $\beta = 15t^{-1}$ this corresponds to $\tau = \frac{1}{6}$). An example is shown below in figure 3(a). The error may be estimated simply as the statistical variation of the running average. In the strong-coupling (but still adiabatic, $\omega_1 < 1$) case the energy of the EP interaction becomes dominant. The parameter which regulates the accuracy of the approximation (18) is now $\alpha = g'\sqrt{h/m\omega} = \tau g_1/\sqrt{\omega_1}$. Consider a typical set of parameters $\beta = 15t^{-1}$, $\omega_1 = 0.3t$ and $g_1 = 1.5$. Even for $M = 150$, which corresponds to a rather small $\tau = 1/10$, one has $\alpha = 0.27$. This is not a very small parameter and the results are expected to change with the further increase of M. This is illustrated in figure 1. The running average for the polaron kinetic energy is shown as a function of the number of measurements for four different values of $M = 150, 180, 210$ and 240. For each value of M two series have been measured. The simulation data exhibit a perfect $1/M^2$-scaling which is seen in figure 2. Extrapolation to $M = \infty$ provides a good estimate for the true value of the kinetic energy for these model parameters. Note that the $M = 150$ result, which corresponds to a rather small $\tau = 1/10$, differs from the correct one by as much as 40%. Measurements of the potential and total energy also reveal the $1/M^2$-dependence. Analogous considerations suggest a scaling at small g_1 but large ω_1. This is indeed the case as shown in figure 3(b). Note that the absolute value of the potential energy is small (since g_1 is small). Nonetheless, the finite-M correction is significant and might lead to large relative errors.

Thus, the systematic study of QMC data as functions of M reveals parameter regions where the M-dependence is significant. In most cases the use of $1/M^2$-scaling enables one to reduce the absolute errors to $\sim 10^{-2}t$. One has to emphasize that this scaling is not usually exploited numerically in QMC studies because this is too time-consuming. It is the efficiency of the present algorithm that allows one to consider very large M and then repeat simulations for several different values of M, all within reasonable computational

time. It should be noted also that the largest $M = 32$ used in reference [22] was apparently too small to reveal the $1/M^2$-scaling. Moreover, a $1/M$-extrapolation scheme was used to estimate the $M \to \infty$ limit. This appears to be incorrect in view of the present research.

The bulk of the numerical results for the two-dimensional Holstein model, presented in the next section, were obtained by the extrapolation procedure described above using four different values of M. These values were usually 90, 120, 150, 180 in the band-electron regime, 120, 150, 180, 210 around the transition to the polaron state, and 150, 180, 210, 240 in the deep-polaronic regime. The temperature was taken as $T = \frac{1}{15}t$. This is a low temperature which ensures that the measured characteristics are close to ground-state properties. For each ω_1, g_1 and M, two series of 150 000 measurements were made. Within a series, successive measurements were taken every M single steps. At the beginning of each series, 10^6 single steps were performed to warm up the system. Sometimes extra series of more measurements were run. Such checks have shown that the results obtained with the settings used are numerically stable. The absolute error of the calculated values is estimated as $(0.01–0.02)t$ at small and large couplings, i.e. away from the transition. Near the transition the error increases up to $(0.10–0.15)t$ due to large statistical fluctuations. In all cases the error is smaller than the size of the symbols used to represent the data.

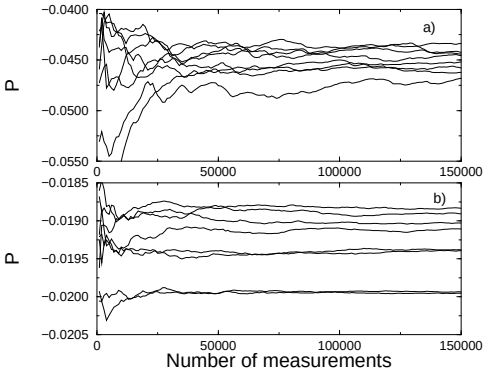

Figure 3. The potential energy in the band-electron regime. (a) $\omega_1 = 0.1$, $g_1 = 0.1$; (b) $\omega_1 = 2.0$, $g_1 = 0.5$. In both cases the measurements were made for $M = 90, 120, 150, 180$. In the latter case (higher frequency) the finite-M scaling is transparent.

4. Numerical results

We begin with the adiabatic regime, $\omega_1 = 0.1$. Note that at such a small frequency, phonons are easy to create and the strong-coupling limit is not accessible using the exact-diagonalization technique [11]. For the QMC method the small frequency is not an obstacle. Figure 4 shows the polaron kinetic, potential and total energies as functions of the reduced coupling constant g_1. At $g_1 = 0$ the potential energy is zero and the total one is very close to the bottom of the free-electron band, $-4t$. For small couplings $g_1 \leqslant 0.2$, all of the energies acquire small corrections which are quadratic in g_1. (This is natural since the coupling enters the trajectory weight as g_1^2; see equation (11).) Note that corrections to the kinetic and potential energies partially compensate each other yielding a correction to the total energy 4–5 times smaller than either of the two.

Around $g_1 \approx 0.25–0.27$ the system changes drastically. For this coupling the kinetic energy increases sharply and the potential one decreases by approximately the same amount.

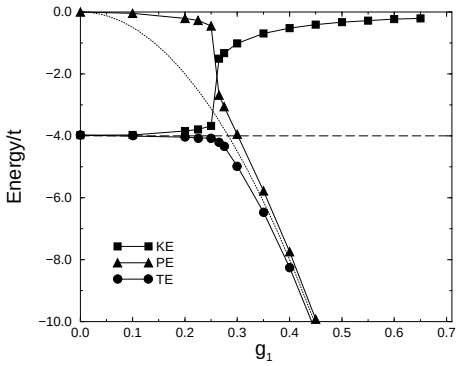

Figure 4. The kinetic, potential and total polaron energies for $\omega_1 = 0.1$. The solid lines are guides to the eye. The bottom of the bare single-electron band is shown by the dashed line. The dotted line indicates the strong-coupling limit for interaction energy, $-E_P = -g_1^2/2\omega_1^2$.

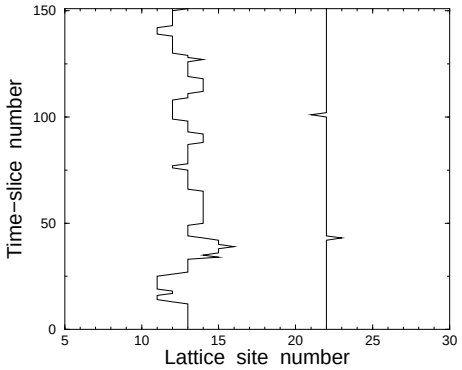

Figure 5. Two typical imaginary-time trajectories: the left-hand one is for the band-electron regime, $g_1 = 0.250$; the right-hand one is for just after the polaron formation, $g_1 = 0.265$. In both cases $\omega_1 = 0.1$, $\beta = 15t^{-1}$ and $M = 150$; cf. figure 4.

This effect is interpreted within the small-polaron picture as follows. In the adiabatic regime the kinetic energy of lattice vibrations is small and the system is governed by the balance between the electron kinetic energy and the energy of the EP interaction (the latter includes the elastic energy of the lattice). The ratio of the two defines the coupling constant λ; see equation (4). At $\lambda \sim 1$ the energy of EP interaction exceeds the kinetic energy and it becomes energetically favourable for the electron to gain a large EP interaction energy and to lose kinetic energy. Accordingly, at this point, oscillators acquire finite displacements from their equilibrium positions resulting in a very rapid decrease of the potential energy by $\simeq 2.2t \sim E_P$. At the same time the electron gets localized in a potential well created by the oscillators which increases its kinetic energy due to the uncertainty principle. The fact that the total energy does not change significantly at the transition shows that the energy is redistributed between kinetic and potential parts suggesting restructuring of the ground state. The path-integral QMC method allows one to visualize such restructuring. Figure 5 compares two typical electron trajectories. The left-hand one was sampled at $g_1 = 0.250$, i.e. just before the polaron formation. It represents a band electron with an extended wave function. The right-hand trajectory was sampled at $g_1 = 0.265$, i.e. after the self-localized state was formed. It is nearly a straight line with rare deviations by one lattice site.

In the small-polaron regime, $g_1 \geqslant 0.265$, the total energy is dominated by the potential contribution which rapidly approaches its strong-coupling limit, $U \to tP \to -E_P = -g_1^2/2\omega_1^2$ (shown in figure 4 by the dotted line). The kinetic energy increases with coupling, suggesting stronger localization of the electron. One should emphasize that the main contribution to the kinetic energy comes from the very fast internal motion of the electron in the potential well and not from the coherent band motion. Therefore the average kinetic energy is not related to the effective mass of the polaron. If fact, the effective mass can be calculated with the QMC method but this amounts to simulating the system with open boundary conditions in imaginary time [30]; see also [25] for the case of the Fröhlich polaron.

Consider now higher phonon frequencies. Figures 6–9 show simulation data for $\omega_1 = 0.3$, 0.5, 1.0 and 2.0 respectively. One can see that the higher the frequency the larger the corrections to the energies in the band-electron regime (small couplings). As a

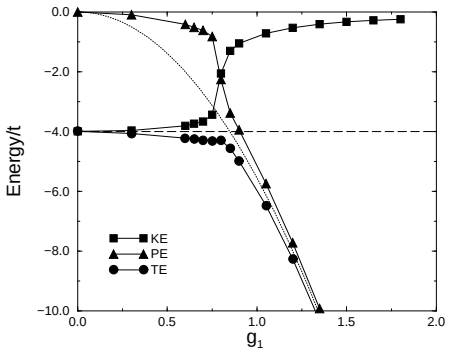

Figure 6. As figure 4, but for $\omega_1 = 0.3$.

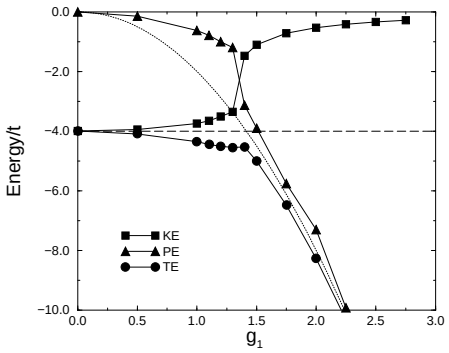

Figure 7. As figure 4, but for $\omega_1 = 0.5$.

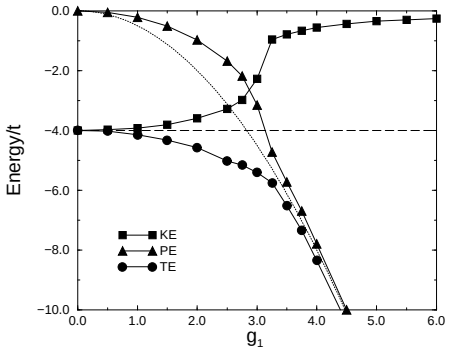

Figure 8. As figure 4, but for $\omega_1 = 1.0$.

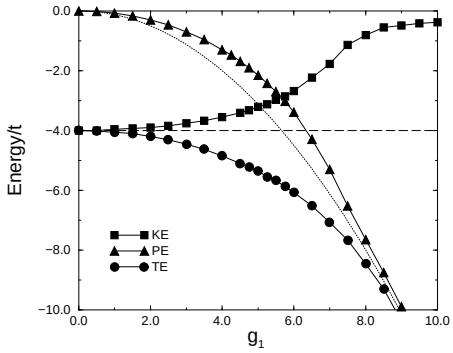

Figure 9. As figure 4, but for $\omega_1 = 2.0$.

result the transition broadens. For $\omega_1 = 1.0$ and 2.0 the transition region is already difficult to locate. At these frequencies the polaron formation is a gradual crossover rather than a sharp transition. Also interesting is that the potential energy approaches the polaron shift as the frequency increases. The polaron shift appears as a natural parameter after the Lang–Firsov transformation [35] of the initial Hamiltonian (1) and characterizes the energy of the EP interaction. Our results show that the approach to the polaron problem based on this transformation becomes adequate in the anti-adiabatic regime.

Apart from the differences near the transition region, figures 4 and 6–9 have different scales of the coupling axis. However, as presented, the data for the adiabatic regime $\omega_1 < 0.5$ look very similar. One notes that the axis scale scales approximately linearly with the frequency. This suggests that thermodynamic properties depend on the ratio of the coupling constant g_1 and the frequency rather than the two parameters separately. A natural physical parameter involving g_1/ω_1 is the coupling constant λ. In figures 10 and 11 the kinetic and potential energies are shown as functions of λ for $\omega_1 = 0.1$, 0.3 and 0.5. One can see that all of the curves are nearly identical in the small-polaron regime, $\lambda \geqslant 1$. The transition moves slightly from $\lambda_{cr} = 0.83 \pm 0.05$ at $\omega_1 = 0.1$ to $\lambda_{cr} = 0.93 \pm 0.05$ at $\omega_1 = 0.5$. By extrapolation we estimate $\lambda_{cr} = 0.80 \pm 0.05$ in the $\omega \to 0$ limit. These results are consistent with a physical expectation that the polaron should form when the energy of the EP interaction exceeds the kinetic energy lost due to localization, i.e. at $\lambda_{cr} \sim 1$. In the band-electron regime the ω_1-dependence is observed; this implies that there are two independent parameters, g_1 and ω_1. For larger frequencies $\hbar\omega = 1.0t$ and $2.0t$

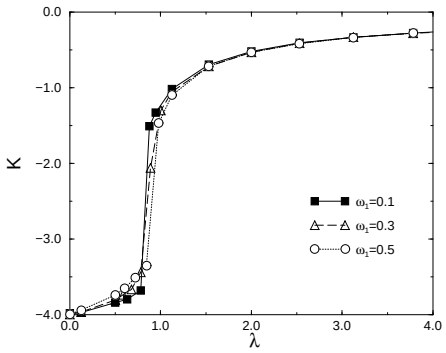

Figure 10. The polaron kinetic energy versus the coupling constant $\lambda = g_1^2/2z\omega_1^2$.

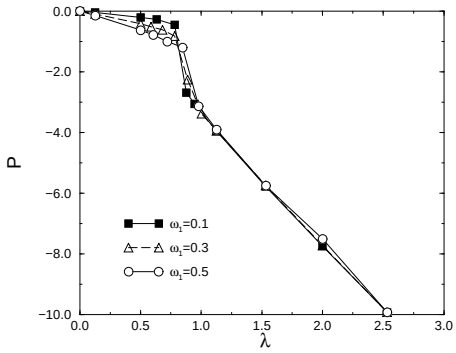

Figure 11. The polaron potential energy versus the coupling constant $\lambda = g_1^2/2z\omega_1^2$.

(not shown in figures 10 and 11), the transition broadens and shifts to $\lambda > 1$. The physical reason for this is that the lattice kinetic energy becomes large for $\hbar\omega > t$. In this case the system is governed by the balance between the lattice energy and the energy of the EP interaction. Then the polaron is expected to form at $g > 1$ which is a stricter condition than $\lambda > 1$ for $\hbar\omega > t$ (see a transparent discussion of the difference between adiabatic and anti-adiabatic regimes in reference [36]). Thus, the polaron transition is expected to move to larger λ and this is exactly what is seen in the QMC results.

5. Conclusions

In this paper we have argued that the quantum Monte Carlo method has definite advantages over other numerical approaches in the study of the long-standing yet unsolved small-polaron problem. The method is not affected by finite-size effects and it is universal for all parameter regions including that of non-zero temperatures. At the same time the temperature can be taken low enough to probe essentially ground-state properties of the system.

In the QMC method only finite numbers of imaginary-time slices M can be studied. We have shown in this paper how this difficulty can be overcome. At big enough M, QMC data exhibit a $1/M^2$-scaling consistent with the accuracy of the symmetric Trotter decomposition. This has enabled us to carry out extrapolation to $M \to \infty$ and to reach very high absolute accuracy $\sim 10^{-2}t$ in the estimation of polaron energetic characteristics.

We have presented results of detailed QMC simulations of the two-dimensional Holstein model. The polaron energy has been calculated as a function of the electron–phonon coupling constant for different phonon frequencies. In the adiabatic regime, $\hbar\omega < t$, the physics is controlled by the balance of the electron kinetic energy and the interaction energy, i.e. by the coupling constant λ. At $\lambda_{cr} \sim 1$ a sharp transition to the small-polaron state occurs. In the limit $\omega \to 0$ the critical coupling is estimated as $\lambda_{cr} = 0.80 \pm 0.05$. At larger frequencies the lattice kinetic energy plays an important role in the energetic balance. The polaron transition broadens and shifts towards larger λ.

Acknowledgments

Part of this work was done at the Department of Physics, King's College London, under the support of EPSRC grant GR/J18675. The author is grateful to A S Alexandrov,

V V Kabanov, E G Klepfish and W Stephan for numerous and helpful discussions on the subject of this paper.

References

[1] Appel J 1968 *Solid State Physics* vol 21, ed F Seitz, D Turnbull and H Ehrenreich (New York: Academic)
[2] Devreese J T (ed) 1972 *Polarons in Ionic Crystals and Polar Semiconductors* (Amsterdam: North-Holland)
[3] Klinger M I 1979 *Problems of Electron (Polaron) Transport Theory in Semiconductors* (Oxford: Pergamon)
[4] Gerlach B and Löwen H 1991 *Rev. Mod. Phys.* **63** 63
[5] Alexandrov A S and Mott N F 1995 *Polarons and Bipolarons* (Singapore: World Scientific)
[6] Devreese J T 1996 *Encyclopedia of Applied Physics* vol 14 (New York: VCH) pp 383–413
[7] Egami T and Billinge S J L 1996 *Physical Properties of High Temperature Superconductors* vol 5, ed D M Ginsberg, p 265
[8] Alexandrov A S and Mott N F 1994 *Rep. Prog. Phys.* **57** 1197
Alexandrov A S and Mott N F 1994 *High-Temperature Superconductors and Other Superfluids* (London: Taylor and Francis) and references therein
[9] Salje E K H, Alexandrov A S and Liang W Y (ed) 1995 *Polarons and Bipolarons in High-T_c Superconductors and Related Materials* (Cambridge: Cambridge University Press)
[10] Ranninger J and Thibblin U 1992 *Phys. Rev.* B **45** 7730
[11] Marsiglio F 1993 *Phys. Lett.* **180A** 280
Marsiglio F 1995 *Physica* C **244** 21
[12] Alexandrov A S, Kabanov V V and Ray D K 1994 *Phys. Rev.* B **49** 9915
[13] Wellein G, Röder H and Fehske H 1996 *Phys. Rev.* B **53** 9666
[14] Stephan W, Capone M, Grilli M and Castellani C 1997 *Phys. Lett.* **227A** 120
[15] Fehske H *et al* 1995 *Phys. Rev.* B **51** 16 582
[16] Stephan W 1996 *Phys. Rev.* B **54** 8981
[17] Zhang C, Jeckelmann E and White S R 1997 *Preprint* cond-mat/9709187
[18] Hirsch J E and Fradkin E 1983 *Phys. Rev.* B **27** 4307
[19] Scalettar R T, Bickers N E and Scalapino D J 1989 *Phys. Rev.* B **40** 197
[20] Marsiglio F 1990 *Phys. Rev.* B **42** 2416
[21] Berger E, Valášek P and von der Linden W 1995 *Phys. Rev.* B **52** 4806
[22] De Raedt H and Lagendijk A 1982 *Phys. Rev. Lett.* **49** 1522
De Raedt H and Lagendijk A 1983 *Phys. Rev.* B **27** 6097
[23] Feynman R P 1955 *Phys. Rev.* **97** 660
Feynman R P 1972 *Statistical Mechanics* (Reading, MA: Benjamin)
[24] Kleinert H 1995 *Path Integrals in Quantum Mechanics, Statistics and Polymer Physics* 2nd edn (Singapore: World Scientific)
[25] Alexandrou C and Rosenfelder R 1992 *Phys. Rep.* **215** 1 and references therein
[26] Metropolis N, Rosenbluth A W, Rosenbluth M N, Teller A H and Teller E 1953 *J. Chem. Phys.* **21** 1987
[27] De Raedt H and Lagendijk A 1984 *Phys. Rev.* B **30** 1671
[28] De Raedt H and Lagendijk A 1985 *Phys. Rep.* **127** 233
[29] De Raedt H and Lagendijk A 1986 *Z. Phys.* B **65** 43
[30] Kornilovitch P E and Pike E R 1997 *Phys. Rev.* B **55** 8634
[31] Holstein T 1959 *Ann. Phys., NY* **8** 325
Holstein T 1959 *Ann. Phys., NY* **8** 343
[32] Trotter H F 1959 *Proc. Am. Math. Soc.* **10** 545
[33] Suzuki M 1976 *Commun. Math. Phys.* **51** 183
[34] Binder K 1979 *Monte Carlo Methods in Statistical Physics* (Berlin: Springer)
Binder K 1992 *Monte Carlo Methods in Condensed Matter Physics* (Berlin: Springer)
[35] Lang I G and Firsov Yu A 1962 *Zh. Eksp. Teor. Fiz.* **43** 1843 (Engl. Transl. 1963 *Sov. Phys.–JETP* **16** 1301)
[36] Capone M, Stephan W and Grilli M 1997 *Phys. Rev.* B **56** 4484